MODELIZATION OF THE SCATTERING OF ELECTROMAGNETIC WAVES FROM THE OCEAN SURFACE

G. Soriano and M. Saillard

Institut Fresnel UMR-CNRS 6133
Faculté des Sciences et Techniques de St Jérôme, Case 162
13397 Marseille Cedex 20, France

Abstract—In this paper, two models for the solution of the electromagnetic bistatic scattering from sea surface are suggested. A rigorous formalism leading to weakly singular integral equations is presented, as well as the surface impedance approximation for low penetrable media and the beam simulation method to synthesize incident beams with arbitrary size. This rigorous integral method is used to test first order approximations, and it is shown that the Small Slope Approximation is very accurate in predicting the scattering cross-section from the high spatial frequencies of the sea surface. This result led us to suggest an improvement of the classical two-scale model, consisting in replacing the small perturbation theory by the small slope approximation. This change allows the cut-off spatial frequency to be shifted so that the use of geometrical Optics is restricted to the large scales.

1. INTRODUCTION

Several applications, like passive remote sensing of ocean brightness temperature [1–3] or the use of GPS signals for active remote sensing [4], require the estimation of the bistatic radar cross-section. In addition, to get significant results about ocean salinity (or soil moisture), the brightness temperature must be estimated with a very high accuracy [5, 6]. Clearly, there is a need for accurate electromagnetic solvers devoted to bistatic scattering from natural surfaces. Even in oceanography, the study of hydrodynamic phenomena for a better description of the sea surface could take advantage of simulated remote sensing experiments with no *electromagnetic bias*. This work should permit one to improve the interpretation and the inversion of microwave remote sensing data from the ocean, the quality of meteorological forecasting and the analysis of exchanges at the air-sea interface.

Thanks to recent improvements of both numerical methods and computers performances, rigorous solution of the three-dimensional electromagnetic scattering from randomly rough surfaces can now be computed. A recent review on this topic has been published in [7]. In time harmonic regime, as far as both the upper and the lower media can be considered as homogeneous, the most efficient methods rely on a boundary integral formalism [8–13]. These methods only differ in the choice of the integral equation and in the way it is numerically solved.

In the microwave frequency range, for given salinity and temperature, sea water can be assumed to be homogeneous. In other words, its electromagnetic properties can be described by a complex permittivity, which also depends on the frequency. Therefore, solving

a surface scattering problem from the sea is of same complexity as from any homogeneous dielectric material, which requires the solution of a set of two coupled integral equations, involving both the electric and magnetic surface current densities. In addition, both the real part and the imaginary part of the permittivity of sea water in the microwave domain is large. Consequently, sea water has a small skin depth, and Green's function in the lower medium exhibits a fast decrease. Such a behaviour can only be captured with the help of a short sampling path, leading to huge linear systems.

To reduce memory requirements and speed up computations, it is assumed that the integral relationship between the electric and magnetic surface currents can be accurately approximated by a local relationship [14]. This kind of approximation, often referred in the literature to as an impedance approximation, or impedance boundary condition, has already been applied to the ocean surface [15, 3]. It has also proved to be very accurate for metallic surfaces in Optics [16], which present a damping rate similar to that of sea water in the microwave domain. It is numerically efficient because the number of unknowns is divided by a factor of two and the fast variations of the field in the lower medium are now included in the local impedance.

However, with our facilities (six 650 MHz PC in parallel), computation times remain very long, typically from days at L band up to weeks at Ku band to get statistically significant results for a single frequency. This is why approximate methods for fast estimating the bistatic cross-section from sea surface are still necessary. But it is important to be able to estimate the accuracy of the various approximate methods through comparisons with rigorous methods.

Our numerical experiments devoted to sea surface spectrum have shown that the scattering patterns have similar shapes for both the impedance approximation and the perfectly conducting model. As a matter of fact, except at large scattering angles, the ratio between the two bistatic cross-sections is close to Fresnel's reflection coefficient. Hence, even though sea water is far from being perfectly conducting, we think this model is well suited for testing approximate methods. Indeed, on one hand computation times with the integral method are divided by a factor of 3 and methods like Kirchhoff approximation are much easier to implement. On the other hand, since a perfectly conducting metal is not dispersive, there is no need to redo the (long) computations for each frequency band. In order to give a great generality to this result, we have also fitted the sea surface spectrum by a power law spectrum. No doubt that the most accurate approximation for sea surface in the microwave range will remain the same than for perfectly conducting surfaces.

Most scattering approximations are basically of high frequency or low frequency type. Since the ocean surface spectrum covers a very wide range of scales, it seems difficult to find a single approximation which applies to all scales. This is why approximate models for sea surface scattering often combine both a high frequency and a low frequency approximation, leading to so-called two-scale models [17, 18]. Consequently, a cut-off frequency separating the two domains has to be chosen. This is a difficult task, since, except for low winds, the domains of validity of the two approximations do not overlap. Therefore, the best choice often results from an optimization based on comparison with real data. To overcome this problem, several attempts have been made to develop approximate methods with domain of validity covering both high and low frequency ranges (the so-called Integral Equation Method [19], the Small Slope Approximation SSA [20], the extended Kirchhoff [21], the Operator Expansion Method [22, 23]). To roughly sum up the great amount of work dedicated to these methods during the last decade, it appears that they all consider the surface slope as a pertinent parameter, and that second order terms in slope are required to fit both small perturbation method for small scales and Kirchhoff approximation for large scales [24]. However, computation of second order terms is a hard task, since it generally involves multiple integration of oscillating functions. This is why in our opinion, there is still interest in studying two scale models combining two methods with low complexity, as first order approximate methods. The aim consists in making the two domains of validity overlap in order to choose the optimal cut-off frequency in this common range.

The paper is organized as follows. In the first part, a rigorous integral formalism leading to weakly singular integral equations is presented, as well as the surface impedance approximation for low penetrable media and the beam simulation method to synthesize incident beams with arbitrary size. The second part of this paper is devoted to testing first order approximations against the rigorous integral method, and it is shown that the Small Slope Approximation is very accurate in predicting the bistatic scattering cross-section from the high spatial frequencies of the sea surface. This result has lead us to suggest an improvement of a classical two-scale model, as described in the last section.

2. RIGOROUS BISTATIC MODEL

Our formulation is based on a surface integral representation of the scattering problem. The case of media with large conductivity such as the ocean surface at microwave frequencies can be modelized by a single

equation thanks to a curved-surface impedance boundary condition. The method of moments (MoM) is then applied, and the resulting linear system is solved by a Sparse Matrix Flat Surface Iterative Approach [25]. The surface, supposed of infinite extent, is illuminated by a Gaussian beam so that only a finite area of the surface has to be considered. However, surfaces of arbitrary area can be handled thanks to the beam decomposition. This technique has been applied to a 410 m long surface with ocean spectrum.

2.1. Surface Integral Representation

We will follow quite closely the notations of Voronovich [20] for the scattering amplitude and the different approximate methods. A rough surface Σ separates the vacuum (upper medium) from an homogeneous (lower) medium of complex relative permittivity ε. We choose the right Cartesian coordinate $(\hat{\mathbf{x}}, \hat{\mathbf{y}}, \hat{\mathbf{z}})$ system with z-axis directed upward and assume Σ is given by an Cartesian equation $z = h(\mathbf{r}) = h(x, y)$. The electromagnetic field is time-harmonic, and an $\exp{(-i\omega t)}$ time dependence is assumed. In vacuum, the field writes as the sum $\mathbf{E}^0 + \mathbf{E}$ of the incident and scattered fields.

The surface Σ needs to be twice continuously differentiable. The unit normal vector $\hat{\mathbf{n}}$ is directed toward vacuum. The tangential components of the electric and magnetic fields on the surface

$$\begin{cases} \mathbf{m} = \hat{\mathbf{n}} \times (\mathbf{E}^0 + \mathbf{E}) \\ \mathbf{j} = \hat{\mathbf{n}} \times (\mathbf{H}^0 + \mathbf{H}) \end{cases} \tag{1}$$

are continuous for a finite relative permittivity ε of the lower medium and satisfy the Statton-Chu integral equations

$$\left(\frac{1}{2} + M^{(1)}\right)\mathbf{m} + \frac{i}{\omega\varepsilon_0}P^{(1)}\mathbf{j} = \hat{\mathbf{n}} \wedge \mathbf{E}^0 \tag{2a}$$

$$\left(\frac{1}{2} + M^{(1)}\right)\mathbf{j} - \frac{i}{\omega\mu_0}P^{(1)}\mathbf{m} = \hat{\mathbf{n}} \wedge \mathbf{H}^0 \tag{2b}$$

and

$$\left(\frac{1}{2} - M^{(2)}\right)\mathbf{m} - \frac{i}{\omega\varepsilon_0\varepsilon}P^{(2)}\mathbf{j} = \mathbf{0} \tag{3a}$$

$$\left(\frac{1}{2} - M^{(2)}\right)\mathbf{j} + \frac{i}{\omega\mu_0}P^{(2)}\mathbf{m} = \mathbf{0} \tag{3b}$$

Superscript (1) (resp. (2)) refers to the upper (resp. lower) medium and M and P are the integral operators introduced by Martin and Ola

in [26]. $\mathbf{R} = \mathbf{r} + h(\mathbf{r})$ and $\mathbf{R'} = \mathbf{r'} + h(\mathbf{r'})$ are two points on Σ, and $\mathbf{c}$ is one of the surface densities $\mathbf{m}$ or $\mathbf{j}$

$$M^{(1,2)}\mathbf{c_R} \quad = \hat{\mathbf{n}}_{\mathbf{R}} \times \mathrm{curl}_{\mathbf{R}} \int_{\Sigma} G^{(1,2)}_{\mathbf{R},\mathbf{R'}} \mathbf{c_{R'}} d\Sigma' \tag{4}$$

$$P^{(1,2)}\mathbf{c_R} \quad = \hat{\mathbf{n}}_{\mathbf{R}} \times \mathrm{curl}_{\mathbf{R}} \mathrm{curl}_{\mathbf{R}} \int_{\Sigma} G^{(1,2)}_{\mathbf{R},\mathbf{R'}} \mathbf{c_{R'}} d\Sigma' \tag{5}$$

The free space Green's function G writes

$$G^{(1,2)}_{\mathbf{R},\mathbf{R'}} = -\exp\left(iK^{(1,2)}|\mathbf{R} - \mathbf{R'}|\right)/4\pi|\mathbf{R} - \mathbf{R'}| \tag{6}$$

with wave numbers $K^{(1)} = K = \omega/c$ for vacuum and $K^{(2)} = \sqrt{\varepsilon}\omega/c$ for the lower medium.

The scattered field can be deduced from the surface densities $\mathbf{m}$ and $\mathbf{j}$, at any point $\mathbf{R} = \mathbf{r} + z\mathbf{z}$ of vacuum:

$$\mathbf{E_R} = -\mathrm{curl}_{\mathbf{R}} \int_{\Sigma} G^{(1)}_{\mathbf{R},\mathbf{R'}} \mathbf{m_{R'}} d\Sigma' - \frac{i}{\omega\varepsilon_0}\mathrm{curl}_{\mathbf{R}}\mathrm{curl}_{\mathbf{R}} \int_{\Sigma} G^{(1)}_{\mathbf{R},\mathbf{R'}} \mathbf{j_{R'}} d\Sigma' \tag{7}$$

2.2. Curved Surface Impedance

The general dielectric problem has two unknown surface densities, but for media with large conductivity, the Green's function (6) of the lower medium shows a fast decreasing behaviour due to $\exp\left(iK^{(2)}|\mathbf{R} - \mathbf{R'}|\right)$ and associated operators M_2 and P_2 have thus short range action. This range is characterized by the skin depth $d = ic/(\omega\sqrt{\varepsilon})$ of the lower medium. An accurate numerical solution of the integral equations (3a) or (3b) would require the currents to be sampled at the skin depth scale. This can be avoided thanks to an impedance approximation: Marvin and Celli in [14] have expanded relationship (3b) between the surface densities as a series with respect to the skin depth d. They have shown that this relationship is local up to the second order: $\mathbf{m} = Z\mathbf{j} + o(d^2)$. So integral relationship (3a) or (3b) can be approximated by a local, impedance-like relationship:

$$\mathbf{m_R} = Z\mathbf{j_R} = \eta\hat{\mathbf{n}}_{\mathbf{R}} \times \left\{ 1 + d\left(\overline{\overline{S}}_{\mathbf{R}} - \frac{tr\left(\overline{\overline{S}}_{\mathbf{R}}\right)}{2}\right) \right\} \mathbf{j_R} \tag{8}$$

$\eta = -i\omega\mu_0 d$ is the intrinsic impedance of the lower medium. Curved surface impedance Z is only function of the skin depth d and of the first and second derivatives of the surface profile at $\mathbf{R}$, i.e., the local

slope and curvature. $\overline{\overline{S}}_{\mathbf{R}}$ denotes the extrinsic curvature tensor, and its trace $tr\left(\overline{\overline{S}}_{\mathbf{R}}\right)$ equals the sum of the surface main curvatures [27].

If the curvature is neglected, one finds back $\mathbf{m_R} = \eta \hat{\mathbf{n}}_{\mathbf{R}} \times \mathbf{j_R}$, a commonly used first order impedance boundary condition [28, 15]. In the limit case of a null skin depth, the impedance approximation gives $\mathbf{m} = \mathbf{0}$, which corresponds to the perfectly conducting surface.

2.3. Method of Moments

Even with an impedance approximation, the surface has to be sampled at the scale of the wavelength in vacuum $\lambda = 2\pi/K$. Thus, the linear system associated by the Method of Moments to a bidimensional surface scattering problem is of large order, and its matrix is full (i.e., non-sparse). This is why:

- the lowest level basis and test functions have been chosen for fast computation of the matrix elements,
- this system is solved in an iterative way, using the Sparse Matrix Flat Surface Iterative Approach [25],
- A Multilevel Canonical Grid technique [11] is used.

2.3.1. Single Weakly Singular Integral Equation

The kernels of operators $M^{(1,2)}$ behave as the first derivative of the Green's functions (4), i.e., as $1/\left|\mathbf{R} - \mathbf{R}'\right|^2$. Pulse functions for basis functions and delta functions for test functions can thus be applied to $M^{(1,2)}$, the singularity of which can be analytically integrated as a Cauchy principal value. Since operators $P^{(1,2)}$ involve one more differentiation (5), they are hypersingular operators, with kernels behaving like $1/\left|\mathbf{R} - \mathbf{R}'\right|^3$. However, this singularity is of electrostatic nature: independent of the wavenumber, it is the same for $P^{(1)}$ and $P^{(2)}$, and so disappears in $\left(P^{(1)} - P^{(2)}\right)$. Summing equations (2b) and (3b) gives a weakly singular integral equation.

$$\left(1 + M^{(1)} - M^{(2)}\right)\mathbf{j} - \frac{i}{\omega\mu_0}\left(P^{(1)} - P^{(2)}\right)\mathbf{m} = \hat{\mathbf{n}} \times \mathbf{H}^0 \qquad (9)$$

The curved surface impedance boundary condition is then applied to get a single unknown integral equation

$$\left[\left(1 + M^{(1)} - M^{(2)}\right) - \frac{i}{\omega\mu_0}\left(P^{(1)} - P^{(2)}\right)Z\right]\mathbf{j} = \hat{\mathbf{n}} \times \mathbf{H}^0 \qquad (10)$$
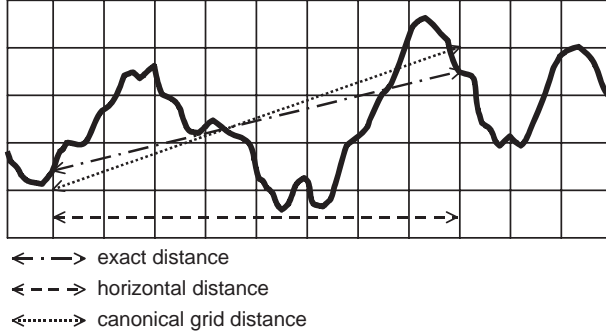
Figure 1. The difference between the exact, the horizontal and the multi-level canonical grid distances.

Therefore the ocean surface scattering problem can be solved using only two unknown scalar functions, as it is the case for the perfectly conducting surface.

The MoM can be applied to equation (10), on a regular 2D-grinding of the (xOy) plane, following [25]. $M^{(2)}$ and $P^{(2)}$ have a short range and Z is local, so they only concern the diagonal elements of the MoM matrix. The equation (10) is more complex than the Magnetic Field Integral Equation for the perfectly conducting surface, so the non-diagonal elements of the MoM matrix are three times longer to compute.

2.3.2. Two Nested Iterative Levels Solver

The MoM system $\mathcal{A}\mathbf{X} = \mathbf{B}$ is solved in an iterative way by the Generalized Minimum Residual algorithm (GMRES). The convergence of this method is greatly sped up by the use of the Sparse Matrix Flat Surface Iterative Approach [25, 29], seen as an iterative preconditioner of the GMRES [13].

The elements of the matrix $\mathcal{A}$ are formally distributed into two matrices $\mathcal{S}$ and $\mathcal{W}$, using a neighborhood distance r_d. The elements corresponding to an interaction at a horizontal distance $|\mathbf{r}_i - \mathbf{r}_j|$ (see Figure 1) smaller than this neighborhood distance r_d constitute the *strong* matrix $\mathcal{S}$, the other elements belonging to the *weak* matrix $\mathcal{W}$.

$$\mathcal{A} = \mathcal{S} + \mathcal{W} : \begin{cases} |\mathbf{r}_i - \mathbf{r}_j| \leq r_d \Rightarrow \mathcal{S}_{ij} = \mathcal{A}_{ij}, \mathcal{W}_{ij} = 0 \\ |\mathbf{r}_i - \mathbf{r}_j| > r_d \Rightarrow \mathcal{S}_{ij} = 0, \mathcal{W}_{ij} = \mathcal{A}_{ij} \end{cases}$$

The neighborhood distance r_d is chosen from physical and numerical criteria, so that the strong matrix $\mathcal{S}$ is a sparse matrix, of which non-

zero elements can be loaded in central memory. Three wavelengths (in vacuum) is a typical value for the neighborhood distance r_d. The product of the weak matrix $\mathcal{W}$ by a vector is handled by the Multilevel Canonical technique, described in the next paragraph.

Due to the short-range coupling effect [30], the strong matrix contains the most important interactions. We choose it as a first approximation of the MoM matrix $\mathcal{A}$, so its inverse can be used as a preconditioning matrix for the GMRES: instead of solving $\mathcal{A}\mathbf{X} = \mathbf{B}$, we consider the (right preconditioned) system $\mathcal{A}\mathcal{S}^{-1}\mathbf{Y} = \mathbf{B}$, which is solved with fewer iterations. When $\mathbf{Y}$ has been found, $\mathbf{X}$ is obtained by solving $\mathbf{Y} = \mathcal{S}\mathbf{X}$.

To solve the system $\mathcal{A}\mathcal{S}^{-1}\mathbf{Y} = \mathbf{B}$, GMRES only requires the computation of the product of the matrix $\mathcal{A}\mathcal{S}^{-1}$ by any vector $\mathbf{U}$. This product is performed in two steps. First, the intermediate system $\mathcal{S}\mathbf{V} = \mathbf{U}$ is solved. Secondly, the product $\mathcal{A}\mathbf{V}$ is computed. Since the matrix $\mathcal{S}$ is sparse and loaded in central memory, the intermediate system $\mathcal{S}\mathbf{V} = \mathbf{U}$ can be quickly solved in an iterative way, with the help of the BiConjugate Gradient Stabilized algorithm.

When the neighborhood distance r_d is large, the flat-surface matrix can be added to the strong matrix $\mathcal{S}$ in the preconditioning process, see [25].

2.3.3. Multi-Level Canonical Grid Technique

The exact computation of the elements of the weak matrix $\mathcal{W}$ is a very time-consuming operation. To overcome this problem, we have implemented the multilevel expansion [11] of the canonical grid method [8]. Let us consider the action of the weak part of an operator M on the surface density $\mathbf{j}$ at $\mathbf{R}_i = \mathbf{r}_i + h(\mathbf{r}_i)\,\hat{\mathbf{z}}$, $\mathbf{R}_i$ corresponding to the node point $\mathbf{r}_i$ of the regular 2D-grinding of the (xOy) plane. It can be expressed as

$$(\mathcal{W}_M\mathbf{j})_i = \hat{\mathbf{n}}_i \wedge \left[\mathbf{R}_i \wedge \left(\sum_j \Gamma_{ij}\mathbf{j}_j \right) - \sum_j \Gamma_{ij} \left(\mathbf{R}_j \wedge \mathbf{j}_j \right) \right] \quad (11)$$

Its evaluation requires the computation of $\mathbf{p}_i = \sum_j \Gamma_{ij}\mathbf{v}_j$. Γ_{ij} is related to the kernel of operator M, and only depends on the exact distance $|\mathbf{R}_i - \mathbf{R}_j|$ when $|\mathbf{r}_i - \mathbf{r}_j| > r_d$.

$$\Gamma_{ij} = \Gamma\left(|\mathbf{R}_i - \mathbf{R}_j|\right) = \delta_x\delta_y \frac{iK\,|\mathbf{R}_i - \mathbf{R}_j| - 1}{|\mathbf{R}_i - \mathbf{R}_j|^2} G_{\mathbf{R}_i,\mathbf{R}_j} \quad (12)$$

As only weak interactions are considered here, Γ_{ij} is null when $|\mathbf{r}_i - \mathbf{r}_j| \leq r_d$.

The $[\min h; \max h]$ interval of the z-axis is regularly sampled. n_z denotes the number of samples and δ_z is the sampling step. Γ_{ij}, as a function of $h(\mathbf{r}_i)$, can be approximated by a Lagrange interpolation $\Gamma_{ij} = \sum_m L_{im}\Gamma(|\mathbf{r}_i + z_m\hat{\mathbf{z}} - \mathbf{R}_j|)$ with coefficients $L_{im} = L_m(h(\mathbf{r}_i))$ [31]. The coefficients of the Lagrange table L are computed once for ever. As Γ_{ij} is also a function of $h(\mathbf{r}_j)$, it can be interpolated on this variable, with the same Lagrange table L. Denoting by $\mathbf{R}_{im} = \mathbf{r}_i + z_m\hat{\mathbf{z}}$, $\mathbf{R}_{jn} = \mathbf{r}_j + z_n\hat{\mathbf{z}}$ and $\Gamma_{imjn} = \Gamma(|\mathbf{R}_{im} - \mathbf{R}_{jn}|)$,

$$\Gamma_{ij} = \sum_{m,n} L_{im}L_{jn}\Gamma_{imjn} \tag{13}$$

$|\mathbf{R}_{im} - \mathbf{R}_{jn}|$ is called the multi-level canonical grid distance (see Figure 1). Product $\mathbf{p}_i$ writes in three steps

$$\mathbf{v}_{jn} = L_{jn}\mathbf{v}_j \tag{14a}$$

$$\mathbf{p}_{im} = \sum_{j,n} \Gamma_{imjn}\mathbf{v}_{jn} \tag{14b}$$

$$\mathbf{p}_i = \sum_m L_{im}\mathbf{p}_{im} \tag{14c}$$

Since $\mathbf{R}_{im}$ and $\mathbf{R}_{jn}$ are nodes of a regular 3D-grid, the matrix Γ_{imjn} can be reindexed in order to become a 3D-Toeplitz matrix. If $n_x n_y$ is the number of points on the 2D-grid, this 3D-Toeplitz matrix is of order $n_x n_y n_z$ and has $(2n_x - 1)(2n_y - 1)(2n_z - 1)$ independent elements. From this matrix, one can build a 3D-circulant matrix of order $2n_x 2n_y 2n_z$, so that one of the submatrices of this 3D-circulant matrix is the original 3D-Toeplitz matrix. A circulant matrix has the property to be diagonal in the Fourier space. The $2n_x 2n_y 2n_z$ diagonal elements of the Fourier transform of the 3D-circulant matrix are computed thanks to a 3D-Fast Fourier Transform and stored in central memory.

The weak part of the operator $\left(P^{(1)} - P^{(2)}\right)$ can be handled in the same way. An expression similar to (11), but more complex, can be given, and the same Lagrange table is used for interpolations.

Each one of the three components of $\mathbf{v}$ (14b) is a $n_x n_y n_z$ vector. Let us consider one of these components. From this vector, a $2n_x 2n_y 2n_z$ vector is build by zero-padding. The 3D-Fast Fourier Transform of this $2n_x 2n_y 2n_z$ vector is computed, the elements of this transform are multiplied by the diagonal elements associated with the matrix Γ_{imjn}, and then an inverse 3D-Fast Fourier Transform is performed. From the resulting $2n_x 2n_y 2n_z$ vector can be extracted the $n_x n_y n_z$ elements of the corresponding component of $\mathbf{p}$ (14b).

Therefore, the complete matrix-vector product (14b) can be achieved at the cost of six 3D-Fast Fourier Transforms of order $2n_x 2n_y 2n_z$ [32].

A precise computation requires a z-axis sampling at the scale of the wavelength in vacuum. The result of the method can be validated by a convergence test, as δ_z tends toward zero. The convergence speed is driven by the interpolation order ℓ. The multi-level canonical grid technique is particularly time-efficient for mildly rough surfaces, where the required number of sampling points on the z-axis is small, typically 8, 16 or 32.

2.4. Scattering Amplitude

In remote sensing, one is concerned by the far field, so formula (7) is not of direct applicability. We recall in this section the scattering amplitude formulation and how it can be extended to incident gaussian beams.

2.4.1. Incident Plane Wave

The scattering amplitude describes the response of the surface in a given direction of space and polarization. Precisely, for an α-polarized incident plane wave of wavevector $\mathbf{K}_0 = \mathbf{k}_0 - q_0\hat{\mathbf{z}}$ and electric field

$$\mathbf{E}_\alpha^0 = q_0^{-1/2} \exp\left(i\mathbf{k}_0 \cdot \mathbf{r} - iq_0 z\right) \hat{\mathbf{p}}_\alpha \qquad (15)$$

the β-polarized component of the scattered field writes:

$$\mathbf{E}_\beta = \int S_{\beta\alpha}(\mathbf{k}, \mathbf{k}_0)\, q^{-1/2} \exp(i\mathbf{k} \cdot \mathbf{r} + iqz)\hat{\mathbf{p}}_\beta \, d\mathbf{k} \qquad (16)$$

Horizontal and vertical components of the wavevectors satisfy $k_0^2 + q_0^2 = K^2$, $q_0 > 0$ and $k^2 + q^2 = K^2$, $\Re e\,(q) + \Im m\,(q) \geq 0$. The factor $q_0^{-1/2}$ is chosen so as to obtain a $\mathbf{k}_0$-independent Poynting vector flow through an horizontal unit surface $(2\omega\varepsilon_0)^{-1}$.

The two-two matrix $S(\mathbf{k}, \mathbf{k}_0) = (S_{\beta\alpha}(\mathbf{k}, \mathbf{k}_0))$ is called the scattering matrix. It is in general expressed in the classical remote sensing VH polarization basis composed of the vertical and horizontal polarizations. Note that the integral of (16) runs over $\mathbb{R}^2$. The components with $k \leq K$ correspond to propagating waves while $k > K$ correspond to evanescent waves. The evanescent waves can be neglected in the far field zone.

2.4.2. Incident Finite Beam

Rather than to describe the incident field by a plane wave, it is more realistic to consider a beam that illuminates only a finite part of the surface. Also, from a numerical point of view, this modelization of the incident field is well suited for the Method of Moments, and it permits one to deal with arbitrarily large surface thanks to the beam superposition method [33]. We will thus assume that the α-polarized electric field is of the form:

$$\mathbf{E}_\alpha^0 = \int\limits_{k_0 \leq K} \tilde{g}(\mathbf{k}_0 - \overline{\mathbf{k}_0}) \, q_0^{-1/2} \exp\left(i\mathbf{k}_0 \cdot \mathbf{r} - iq_0 z\right) \hat{\mathbf{p}}_\alpha \, d\mathbf{k}_0 \qquad (17)$$

A common choice for the spectral amplitude function $\tilde{g}$ is a Gaussian beam with widths $1/\ell_x$, $1/\ell_y$:

$$\tilde{g}\left(\mathbf{k}\right) = \sqrt{\frac{\ell_x \ell_y}{\pi}} \exp\left(-\frac{\ell_x^2 k_x^2 + \ell_y^2 k_y^2}{2}\right) \qquad (18)$$

The characteristic sizes of the beam footprint on the surface are then ℓ_x, ℓ_y. $\overline{\mathbf{k}_0}$ denotes the mean incident direction of the beam. The scattered field writes

$$\mathbf{E}_\beta \;\; = \;\; \int \bar{S}_{\beta\alpha}(\mathbf{k}, \overline{\mathbf{k}_0}) \, q^{-1/2} \exp(i\mathbf{k} \cdot \mathbf{r} + iqz)\hat{\mathbf{p}}_\beta \, d\mathbf{k} \quad (19)$$

$$\bar{S}_{\beta\alpha}(\mathbf{k}, \overline{\mathbf{k}_0}) \;\; = \;\; \int\limits_{k_0 \leq K} \tilde{g}(\mathbf{k}_0 - \overline{\mathbf{k}_0}) \, S_{\beta\alpha}(\mathbf{k}, \mathbf{k}_0) \, d\mathbf{k}_0 \qquad (20)$$

Applying Weyl's transformation to (7) and identifying with (19), we obtain

$$\bar{S}_{\beta\alpha}(\mathbf{k}, \overline{\mathbf{k}_0}) \;\; = \;\; -\frac{Kq^{-1/2}}{8\pi^2} \int_\Sigma \left[\left(\hat{\mathbf{p}}_\beta \times \hat{\mathbf{K}}\right) \cdot \mathbf{m}_\mathbf{R}^\alpha + \sqrt{\frac{\mu_0}{\varepsilon_0}}\hat{\mathbf{p}}_\beta \cdot \mathbf{j}_\mathbf{R}^\alpha\right]$$
$$\exp(-i\mathbf{k} \cdot \mathbf{r} - iqz)d\Sigma \qquad (21)$$

with scattered wavevector $\mathbf{K} = \mathbf{k} + q\hat{\mathbf{z}}$ and unit vector $\hat{\mathbf{K}} = K/K$. $\mathbf{m}^\alpha$ and $\mathbf{j}^\alpha$ are the solutions of integral equations for the incident field (17).

    The incident and scattered energy can be defined as the flux of the Poynting vector through a horizontal plane $z = z_m$ above the surface (i.e., $z_m > \max h$). Using Parseval's formula, this leads to integrals in the spectral domain for the incident and scattered energies

$$\Phi_\alpha^0 \;\; = \;\; \frac{1}{2\omega\varepsilon_0} \int\limits_{k_0 \leq \omega/c} \left|\tilde{g}(\mathbf{k}_0 - \overline{\mathbf{k}_0})\right|^2 d\mathbf{k}_0 = \frac{1}{2\omega\varepsilon_0} = \Phi^0 \qquad (22)$$

$$\Phi_{\beta\alpha} \quad = \quad \Phi^0 \int\limits_{k \le \omega/c} \left| \bar{S}_{\beta\alpha}(\mathbf{k}, \mathbf{k}_0) \right|^2 \, d\mathbf{k} \tag{23}$$

The normalized scattered intensity is thus defined as

$$I_{\beta\alpha} = \frac{d\Phi_{\beta\alpha}}{\Phi^0 d\Omega} = Kq \left| \bar{S}_{\beta\alpha} \right|^2 \tag{24}$$

In the vicinity of normal incidence, we use a specific polarization basis rather than the VH:

$$\begin{cases} \hat{\mathbf{p}}_E = \mathbf{k} \times \mathbf{y}/ \|\mathbf{k} \times \mathbf{y}\| \\ \hat{\mathbf{p}}_H = \hat{\mathbf{K}} \times \hat{p}_E \end{cases} \tag{25}$$

Note that $(\hat{\mathbf{p}}_E, \hat{\mathbf{p}}_H)$ coincides with $\left(\hat{\mathbf{v}}, \hat{\mathbf{h}} \right)$ in the mean incidence plane.

2.5. Beam Decomposition and Parallel Computations

2.5.1. The Beam Decomposition Method

At this stage, the scattered field can be computed numerically, but for small beam footprints only. As a matter of fact, the random access memory required by the MoM grows linearly with the illuminated area and the computing time increases even faster, so that the footprint that can be handled with common numerical facilities is of some wavelengths radius. This footprint is several orders smaller than a real remote sensing measurement footprint.

Beam decomposition is an elegant way to reconcile real experiments and MoM. It has originally been developed for one-dimensional random rough surfaces [33], but adaptation to two-dimensional surfaces is straightforward [13]. Beam decomposition is based on the representation of a *large* beam by a weighted sum of shifted *narrow* beams. Each narrow beam is handled as a particular scattering problem. Summing the scattering amplitudes from all the narrow beams provides the scattering amplitude from the large one.

Following paragraph 2.4.2, the incident large beam is characterized by dimensions ℓ_x and ℓ_y. In a similar way, the incident narrow beams have dimensions $n_x < \ell_x$ and $n_y < \ell_y$. The scattering amplitude $\bar{S}_{\alpha\beta}$ of the large beam is expressed from the scattering amplitudes $\bar{S}_{\alpha\beta}^{nm}$ of the narrow beams:

$$\bar{S}_{\alpha\beta} \left(\mathbf{k}, \overline{\mathbf{k}_0} \right) = \sum_{n=-N_n}^{N_n} \sum_{m=-N_m}^{N_m} u_{nm} \left(\mathbf{k} - \overline{\mathbf{k}_0} \right) \bar{S}_{\alpha\beta}^{nm} \left(\mathbf{k}, \overline{\mathbf{k}_0} \right) \tag{26}$$

where $\mathbf{r}_{nm} = (n\Delta X, m\Delta Y)$ and

$$u_{nm}\left(\mathbf{k}\right) = \frac{\Delta X \Delta Y}{2\pi} \frac{\exp\left(-i\mathbf{k}\cdot\mathbf{r}_{nm}\right)}{\sqrt{\ell_x^2 - n_x^2}\sqrt{\ell_y^2 - n_y^2}} \exp\left[-\frac{1}{2}\left(\frac{(n\Delta X)^2}{\ell_x^2 - n_x^2} + \frac{(m\Delta Y)^2}{\ell_y^2 - n_y^2}\right)\right]$$
(27)

Numerical experimentation has shown that a good representation of the large beam is achieved with an overlapping $\Delta X \simeq 2n_x$ and $\Delta Y \simeq 2n_y$.

In order to modelize a real measurement, the computed scattered intensity (24) might have to be averaged over the angular aperture of the receive antenna. Otherwise, the scattering pattern is oscillating with a characteristic period equal to the angular width of the incident beam.

The beam decomposition is naturally well fitted for parallel computation. As a matter of fact, after the rough surface is divided and weights for the decomposition are evaluated, the following tasks (computation of the incident field on the surface, building the matrices, solving the system and computing the scattering amplitude) can be performed independently for each narrow beam. Then, scattering amplitudes need only be summed. This scheme is particularly adapted to distributed memory parallel environment.

The overlapping between narrow beams ensures that interactions between adjacent beams are taken into account. Further interactions are neglected. Another limitation of the beam decomposition is that the maximum incident angle is given by the size of the narrow beam. Grazing angles are still a tricky problem.

2.5.2. Application to a 410 m Long Perfectly Conducting Surface with Ocean Spectrum

We consider the unified ocean spectrum proposed in [34]. Figure 2 shows the omnidirectional spectrum $S(\kappa)$ and the spreading delta ratio $\Delta(\kappa)$ of the directional spectrum

$$\Psi\left(\kappa_x, \kappa_y\right) = \Psi\left(\kappa, \phi\right) = \frac{S(\kappa)}{\kappa}\frac{1 + \Delta(\kappa)\cos\left(2\phi\right)}{2\pi} \tag{28}$$

for a wind speed of $10\,\mathrm{m/s}$ at a height of $10\,\mathrm{m}$. This spectrum includes spatial wavelengths as low as $1.5\ 10^{-2}\,\mathrm{rad/m}$, whereas the lowest electromagnetic wavenumber used in ocean remote sensing is $30\,\mathrm{rad/m}$ (L band, $\lambda = 0.2\,\mathrm{m}$). In these conditions, the minimum beam footprint size to cover the whole spectrum is two thousand wavelengths. Therefore, we have considered a 2048λ long, that is $410\,\mathrm{m}$
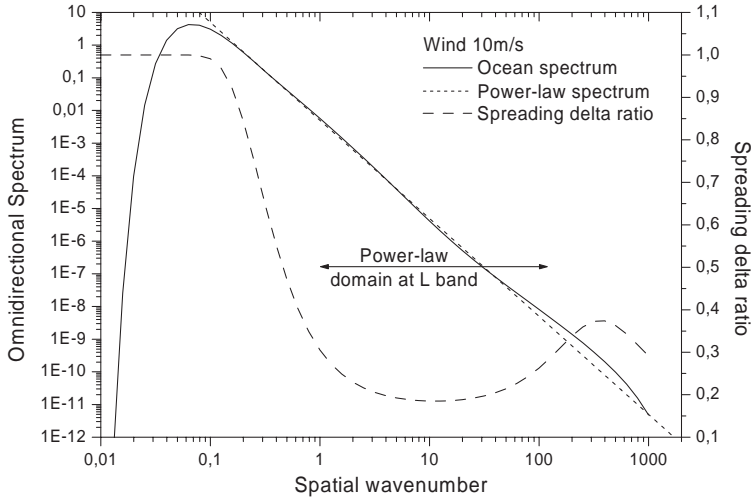
Figure 2. Omnidirectional spectrum S and spreading delta ratio Δ of the Unified ocean spectrum against spatial wavenumber κ for a wind speed of $10\,\mathrm{m/s}$ at a height of $10\,\mathrm{m}$. The horizontal arrow represents a spatial wavelength domain around the L band electromagnetic wavenumber where the power-law spectrum fits the the ocean spectrum.

long surface, sampled at $\delta_x = \delta_y = 2.5\,\mathrm{cm}$. The beam decomposition technique is applied to narrow beams illuminating square surfaces of $16\lambda = 3.2\,\mathrm{m}$ side and centered on the x-axis. With an overlapping of $\Delta X = 12\lambda = 2.4\,\mathrm{m}$, 509 narrow beams have to be lined up in order to synthesize a $410\,\mathrm{m}$-long large beam. Since this beam is only $3.2\,\mathrm{m}$-large, the anisotropy of the ocean spectrum cannot be correctly taken into account, and the delta ratio has been set to zero. Incidence is normal and the electric field is parallel to the length of the surface.

Figure 3 shows the fast-oscillating scattering pattern given by the beam decomposition for a perfectly conducting surface. The smooth curves have been obtained by averaging the scattered intensity (24) over a $10°$ aperture.

3. TESTING APPROXIMATE METHODS

3.1. Description of the Surface

In this section, our goal is to test the most common first order approximate methods on the ocean surface. However, the ocean surface
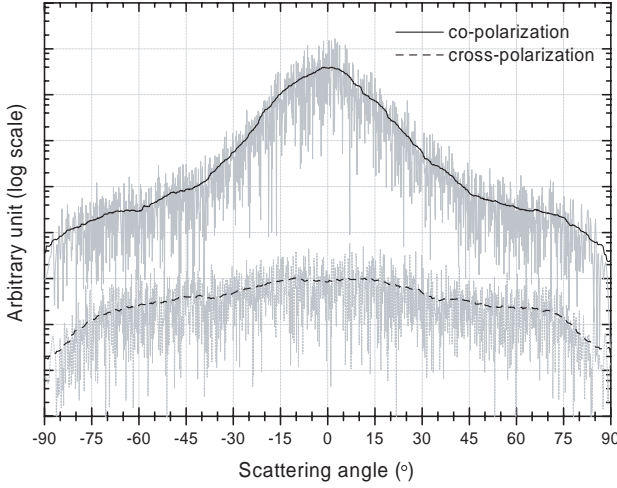
Figure 3. Non-normalized scattered intensity against scattering angle for a 410 m long perfectly conducting surface with ocean spectrum at L band and normal incidence. The smooth curves have been obtained by averaging over a $10°$ aperture.

spectrum and permittivity depend on many parameters, among which the wind speed and direction, the electromagnetic wavelength, the salinity and the temperature. As the MoM computations are very time-consuming, we feel the need to give the most universal value to each computation.

For a given electromagnetic wavenumber K, the ocean spectrum decays fast enough in order to ensure that high-wavenumbers $\kappa > \kappa_u \gg K$ do not contribute to the scattering process. We have set $\kappa_u/K = 4$, which has been shown numerically in the 1D case to be the electromagnetic cut-off. We also choose a low-wavenumber cutoff $\kappa_l \ll K$ and consider the band-limited power-law spectrum:

$$\Psi_r\left(\kappa\right) = \begin{cases} \alpha\,\kappa^{-4} & \kappa \in [\kappa_l; \kappa_u] \\ 0 & \kappa \notin [\kappa_l; \kappa_u] \end{cases} \tag{29}$$

This spectrum has two remarkable features.

- First, for given values of κ_u/K and κ_l/K, neither $K\sigma$ nor s, the zeroth and second moments of the spectrum, depend on K:

$$\begin{cases} K\sigma = \sqrt{\alpha/2}\sqrt{(\kappa_l/K)^{-2} - (\kappa_u/K)^{-2}} \\ s = \sqrt{\alpha\ln\left(\kappa_u/\kappa_l\right)} \end{cases} \tag{30}$$
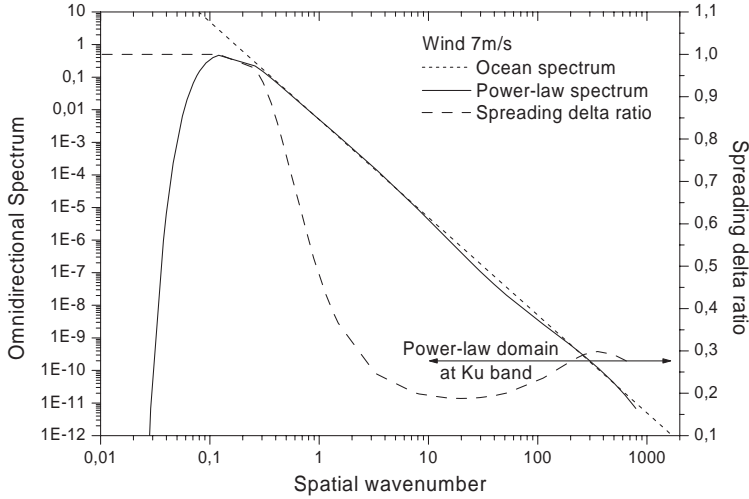
Figure 4. Omnidirectional spectrum S and spreading delta ratio Δ of the Unified ocean spectrum against spatial wavenumber κ for a wind speed of $7\,\text{m/s}$ at a height of $10\,\text{m}$. The horizontal arrow represents a spatial wavelength domain around the Ku band electromagnetic wavenumber where the power-law spectrum fits the the ocean spectrum.

- Secondly, with a multiplicative factor set to $\alpha = 5.25\ 10^{-3}$ and for a low-wavenumber cutoff κ_l/K as low as $1/30$, this spectrum correctly fits the ocean omnidirectional spectrum on $[\kappa_l; \kappa_u]$ for various values of the electromagnetic wavenumber and wind speed. Consider for example the L band for a $10\,\text{m/s}$ wind speed (Figure 2) and the Ku band for a $7\,\text{m/s}$ wind speed (Figure 4). Moreover, as the delta ratio is generally small on $\kappa \in [K/30; 4K]$, the truncated power-law spectrum is representative of the ocean directional spectrum on this domain of κ.

Hence, considering this spectrum and assuming there is no dependency of ε on K, the scattered field for various electromagnetic wavenumbers and winds can be obtained through one computation. In a first step, the surface is thus assumed to be perfectly conducting. This is justified by the high value of the conductivity of the ocean surface, and this will enable us to discriminate the different approximate methods.

3.2. Perfectly Conducting Ocean Surface

One of the most popular approximation in scattering from rough surfaces is the Kirchhoff Approximation (KA), also known as the Tangent Plane or Physical Optics approximation. It is known to be valid when the incident wavelength is small compared to the correlation length of the surface. The Small Slope Approximation (SSA), first introduced in [20], starts from an ansatz based on the invariance properties of the scattering amplitude for an incident plane wave. Performing a horizontal or vertical translation $\mathbf{d}$ on the surface only affects the latter by a phase shift $\exp\left(-i\left(\mathbf{k}-\mathbf{k}_0\right)\cdot\mathbf{d}\right)$ or $\exp\left(-i\left(q+q_0\right)\hat{\mathbf{z}}\cdot\mathbf{d}\right)$, respectively, so that a solution is sought in the form:

$$S(\mathbf{k},\mathbf{k}_0)=\frac{1}{(2\pi)^2}\int d\mathbf{r}\,\exp\left(-i\left(\mathbf{k}-\mathbf{k}_0\right)\cdot\mathbf{d}-i\left(q+q_0\right)h\left(\mathbf{r}\right)\right)\Xi\left[\mathbf{k},\mathbf{k}_0,\mathbf{r},h\right],$$

where Ξ is some functional that contains the explicit dependence on the surface ($\Xi=1$ for the plane). The unknown Ξ is obtained by performing a functional Taylor expansion with respect to the Fourier transform $\tilde{h}$ and imposing the coefficients to be consistent with the Small Perturbation Method (SPM) as $h\to0$. The first order approximation for KA and SSA can be summarized in the following formula [20, pp. 123 and 154]

$$S(\mathbf{k},\mathbf{k}_0)=B(\mathbf{k},\mathbf{k}_0)\frac{2\sqrt{qq_0}}{q+q_0}\frac{1}{(2\pi)^2}\int d\mathbf{r}\,\exp\left(-i\left(\mathbf{k}-\mathbf{k}_0\right)\cdot\mathbf{r}-i\left(q+q_0\right)h\left(\mathbf{r}\right)\right)$$

$$(31)$$

where the matrix $B(\mathbf{k},\mathbf{k}_0)$ is given by

$$B_{KA}(\mathbf{k},\mathbf{k}_0)=\frac{1}{2qq_0}\begin{bmatrix}\left(K^2+qq_0\right)\hat{\mathbf{k}}\cdot\hat{\mathbf{k}}_0-kk_0 & K\left(q+q_0\right)\hat{\mathbf{z}}\cdot\left(\hat{\mathbf{k}}\times\hat{\mathbf{k}}_0\right)\\ K\left(q+q_0\right)\hat{\mathbf{z}}\cdot\left(\hat{\mathbf{k}}\times\hat{\mathbf{k}}_0\right) & -\left(K^2+qq_0\right)\hat{\mathbf{k}}\cdot\hat{\mathbf{k}}_0+kk_0\end{bmatrix}$$

$$(32)$$

for the KA and

$$B_{SPM}(\mathbf{k},\mathbf{k}_0)=\frac{1}{qq_0}\begin{bmatrix}K^2\hat{\mathbf{k}}\cdot\hat{\mathbf{k}}_0-kk_0 & Kq_0\,\hat{\mathbf{z}}\cdot\left(\hat{\mathbf{k}}\times\hat{\mathbf{k}}_0\right)\\ Kq\,\hat{\mathbf{z}}\cdot\left(\hat{\mathbf{k}}\times\hat{\mathbf{k}}_0\right) & -qq_0\hat{\mathbf{k}}\cdot\hat{\mathbf{k}}_0\end{bmatrix}$$

$$(33)$$

for the SSA. Note that the KA and SSA at first order differ only by the geometrical factor $B(\mathbf{k},\mathbf{k}_0)$, that does not depend on the roughness. The off-diagonal terms of the scattering matrix vanish when $\hat{\mathbf{k}}=\hat{\mathbf{k}}_0$, meaning that no depolarization occurs in the incidence plane. In the specular direction ($\mathbf{k}=\mathbf{k}_0$), the upper and lower diagonal elements for

both approximations reduce to $+1$ and -1, respectively. In the limit $h \to 0$, the complex exponential in the integrand can be linearized, yielding to:

$$S(\mathbf{k}, \mathbf{k}_0) = B_{SPM}(\mathbf{k}, \mathbf{k}_0) \left(\delta(\mathbf{k} - \mathbf{k}_0) - 2i\sqrt{qq_0} \frac{\tilde{h}(\mathbf{k} - \mathbf{k}_0)}{(2\pi)^2} \right) \qquad (34)$$

which is the classical formula of SPM when $B(\mathbf{k}, \mathbf{k}_0)$ is given by (33).

The computation of the scattering amplitude for a finite beam $\bar{S}_{\beta\alpha}$ in the KA or SSA after (20) and (31) involves a double summation over the space and frequency variable $\mathbf{r}$ and $\mathbf{k}_0$, respectively, which becomes computationally demanding in the 3D case. However, the computation can be greatly simplified by assuming that the finite beam is sufficiently narrow (spectrally), so that we may approximate $B(\mathbf{k}, \mathbf{k}_0) \simeq B(\mathbf{k}, \overline{\mathbf{k}_0})$ and $q_0 \simeq \overline{q_0}$ within the beam and extend the $\mathbf{k}_0$ domain of integration to infinity. In that case, the integral over $\mathbf{k}_0$ is a mere inverse Fourier transform of the beam envelope $\tilde{g}$, which leads to:

$$\bar{S}(\mathbf{k}, \overline{\mathbf{k}_0}) = B(\mathbf{k}, \overline{\mathbf{k}_0}) \frac{2\sqrt{qq_0}}{q + q_0} \int d\mathbf{r} \, g(\mathbf{r}) \exp\left(-i(\mathbf{k} - \mathbf{k}_0) \cdot \mathbf{r} - i(q + q_0) h(\mathbf{r})\right)$$
$$(35)$$

This expression becomes accurate as the wavelength becomes small compared to the beam size, $\lambda \ll \ell_x, \ell_y$, or equivalently as the wavenumber becomes much larger than the spectral width, $K \gg 1/\ell_x, 1/\ell_y$. The scattering amplitude for a finite beam $\bar{S}_{\beta\alpha}$ in the SPM is directly obtained applying (20) on (34).

Figure 5 show Monte-Carlo simulations of the scattering intensity for the KA, the SSA, the SPM and the MoM. The ensemble average has been performed over 1000 sample surfaces for the approximate methods and 100 sample surfaces (due to the large computation time) for the MoM.

Both KA and SSA turn out to be extremely accurate (less than .5 dB error) in both polarizations for small angles ($-30° \le \theta \le +50°$), but only SSA remains reliable over the whole range of scattering angles (less than 1 dB error in VV and for $-65° \le \theta \le +75°$ in HH). SPM surestimates by far the scattering coefficient in the specular region but becomes reliable at larger angles as it meets the SSA. The only reproach we can make on SSA is that it doesn't vanish with q for the V polarisation.

Hence, the SSA appears to be the only first order approximate method to give an accurate estimation of the whole scattering pattern of the ocean spectrum with a low-wavenumber cutoff κ_l as low as $K/30$.
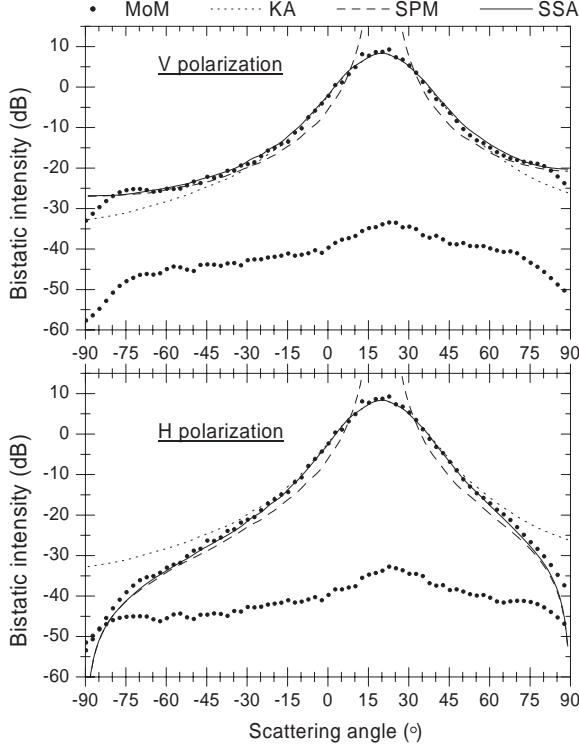
Figure 5. Normalized scattered intensity against scattering angle for a perfectly conducting surface with band-limited power-law spectrum at 20° incidence.

3.3. SSA for the Dielectric Ocean Surface

As applied to perfectly conducting or dielectric surfaces, SSA only differ by the geometrical factor $B(\mathbf{k}, \mathbf{k}_0)$. For a relative permittivity ε, the SPM gives

$$
B_{SPM}^{\varepsilon}(\mathbf{k}, \mathbf{k}_0) = (\varepsilon - 1)
\begin{bmatrix}
\dfrac{q^{(2)} q_0^{(2)} \hat{\mathbf{k}} \cdot \hat{\mathbf{k}}_0 - \varepsilon k k_0}{\left(\varepsilon q + q^{(2)}\right)\left(\varepsilon q_0 + q_0^{(2)}\right)} & \dfrac{K q_0^{(2)} \hat{\mathbf{z}} \cdot \left(\hat{\mathbf{k}} \times \hat{\mathbf{k}}_0\right)}{\left(q + q^{(2)}\right)\left(\varepsilon q_0 + q_0^{(2)}\right)} \\[4mm]
\dfrac{K q^{(2)} \hat{\mathbf{z}} \cdot \left(\hat{\mathbf{k}} \times \hat{\mathbf{k}}_0\right)}{\left(\varepsilon q + q^{(2)}\right)\left(q_0 + q_0^{(2)}\right)} & \dfrac{K^2 \hat{\mathbf{k}} \cdot \hat{\mathbf{k}}_0}{\left(q + q^{(2)}\right)\left(q_0 + q_0^{(2)}\right)}
\end{bmatrix}
\tag{36}
$$

with $q_0^{(2)} = \sqrt{\varepsilon K^2 - k_0^2}$ and $q^{(2)} = \sqrt{\varepsilon K^2 - k^2}$.

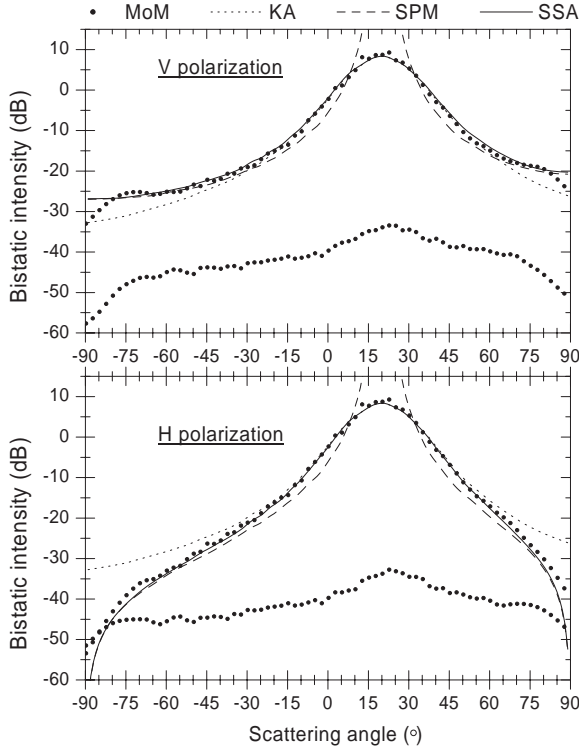In Figure 6 we have plotted the Monte-Carlo simulations of the

Figure 6. Normalized scattered intensity against scattering angle for a dielectric surface with band-limited power-law spectrum and permittivity $\varepsilon = 73.5039 + i60.9670$ at $20°$ incidence.

scattering intensity for the SSA and the MoM. Relative permittivity has been set to $\varepsilon = 73.5039 + i60.9670$, which is the value at L band for a sea surface temperature of $15°C$ and a salinity of 35 psu, following [35]. Figure 6 shows that the SSA is perfectly reliable. It appears that SSA is even better for a finite permittivity: the scattered intensity is of remarkable agreement with MoM, even for low grazing angles in V polarization.

4. AN IMPROVED BISTATIC TWO-SCALE MODEL

Let us consider again the application of the beam decomposition technique on a 410 m long ocean surface (Section 2.5.2). The scattering amplitudes of the 509 narrow beams have been summed following (27), the scattering intensity has been computed and averaged over
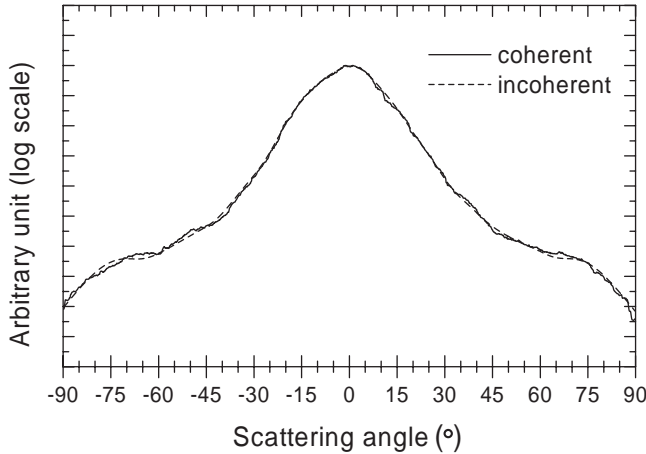
Figure 7. Non-normalized scattered intensity against scattering angle for 509 narrow beams illuminating a 410 m long perfectly conducting ocean surface at L band and normal incidence. Comparison between the coherent (beam decomposition) and the incoherent sum.

a 10° aperture. The 509 scattering computations could be combined in another way. Instead of summing the scattering amplitudes, one first computes the 509 scattering intensities from the weighted scattering amplitudes, and then sums all the contributions. This incoherent pattern, which has the 10° angular aperture of the narrow beams, coincide (Figure 7) with the angular averaged coherent pattern (beam decomposition). Roughly speaking, this numerical example shows that, illuminating an ocean surface of very large extent or scanning this surface with a small beam leads to the same scattering intensity pattern. Since the small beams cannot capture the low frequency behaviour of the surface power spectrum, this numerical experiment makes us think that the influence of the large scales on the scattering pattern may be accurately taken into account through simple geometrical considerations. This idea has been developed for a long time [17, 36] and has given birth to a class of models referred to as two-scale models. By two-scale model, we mean an electromagnetic model dealing separately with the *high* and *low* spatial frequencies. This requires the power spectrum of the surface to be divided into these two kind of scales, including the choice of a cut-off frequency.

The simplest two-scale model, from a conceptual point of view, combines the small perturbation theory with geometrical Optics [17]. Basically, the scattering problem is replaced by that of a small

scale roughness illuminated under some local incidence angle and polarization state related to the local slope. Averaging over the density of probability of slopes, derived from the low frequency part of the surface spectrum, provides the scattering cross-section from the sea surface. The use of the small perturbation theory for predicting the small scales contribution drastically limits the choice of the cut-off spatial frequency. Indeed, if one admits that the upper bound of the domain of validity of perturbation theory in terms of root mean square height is roughly given by $K\sigma = 0.3$, the lowest cut-off frequency is $\kappa_c = K/6$ with the surface spectrum considered in the previous section. As a consequence, geometrical Optics approximation is applied as soon as $\kappa < K/6$, which in our opinion is quite a high spatial frequency. Nevertheless, this model has been widely implemented and tested over the past decades, and it seems that the optimal cut-off lies between $K/2$ and $K/3$ for estimation of the backscattering cross-section [37, 38].

The numerical results from the previous section have naturally lead us to suggest a new two-scale model for fast computation of the bistatic cross-section from sea surface. It simply consists in replacing the small perturbation theory by the first-order small slope approximation to describe the contributions from the high spatial frequencies in the two-scale model described above. The previous section clearly shows that the cut-off between the high and low frequency approximations can be moved very far towards the low spatial frequency range, down to $K/30$ at least. Not only thinking in terms of rays in the range $\kappa < K/30$ (instead of $K/3$) is much more reasonable, but first order small slope approximation in the range $\kappa > K/30$ is also more accurate than first order small perturbation method in the range $\kappa > K/3$, especially around the specular reflection direction.

Our computations have been restricted to isotropic surfaces, though obviously sea surface is not isotropic. However, as noticed in Section 3.1, the delta ratio, which is a measure of surface anisotropy at each scale, remains rather low in the high frequency range. Therefore, as a first approximation, we suggest to neglect the surface anisotropy above the low frequency cut-off. Moreover, from the theoretical point of view, this approximation can be removed and anisotropy could be taken into account in a more complete model. Of course, the cut-off suggested in this paper remains arbitrary. It results from the restriction of our rigorous computations to surface samples which could not include larger scales. May be first order mall-slope approximation remains accurate over a wider spatial frequency range, but one has to take care of surface anisotropy in this case.

More sophisticated, but more difficult to implement, two-scale

models have been proposed. For instance, Bass and Fuks [36] suggest to apply the small perturbation method to a smooth underlying surface described by the low spatial frequencies. This method requires the computation of Green's dyadics for a half-space bounded by such a smooth surface. This can be achieved thanks to Kirchhoff approximation. However, a similar combination involving Kirchhoff approximation for large scales and small slope approximation for small scales is not straightforward, since the derivation of the scattering amplitudes with small slope approximation does not result from the convolution product of some Green's function with some surface density. As an improvement of this model, we could suggest to perform a rigorous computation of the perturbation induced by the small scale roughness when superimposed to large scales. This would also permit one to move down the cut-off frequency but would require huge computation times.

It must be noticed that all the models discussed in this section assume long range interactions to be negligible. In other words, multiple reflections induced by large scales are neglected. Indeed, the *rigorous* model is limited by the size of the elementary beams, while geometrical Optics and first order Kirchhoff approximation do not include multiple scattering. The accuracy of this assumption is not estimated here.

5. CONCLUSION

In this paper, two models for the solution of the electromagnetic scattering from sea surface are suggested. One is based on a rigorous integral formalism, combined with an impedance approximation and the beam simulation technique. It is aimed at providing an accurate simulation of a real remote sensing experiment from sea surface. Since computation times are by far much too long for practical applications with such a model, fast approximate models are required. Therefore, the *rigorous* model has been used to estimate the accuracy of various approximations. This study led us to suggest an improvement of the classical two-scale model, consisting in replacing the small perturbation theory by the small slope approximation. This suggestion is supported by rigorous computations showing a perfect agreement between the numerical simulations and the small slope approximation for surface samples with root mean square height far beyond the domain of validity of the small perturbation method. This change allows the cut-off spatial frequency to be divided by a factor close to ten, which restricts the use of geometrical optics to large scales ($\kappa < K/30$).

REFERENCES

1. Tsang, L., J. A. Kong, and T. Shin, *Theory of Microwave Remote Sensing,* Wiley-Interscience, New York, 1985.

2. Johnson, J. T. and M. Zhang, "Theoretical study of the small slope approximation for ocean polarimetric thermal emission," *IEEE Trans. Geosci. Remote Sensing,* Vol. 37, 2305–2316, 1999.

3. Zhou, L., L. Tsang, V. Jandhyala, and C. T. Chen, "Studies on accuracy of numerical simulations of emission from rough ocean-like surfaces," *IEEE Trans. Geosci. Remote Sensing,* Vol. 39, 1757–1763, 2001.

4. Fung, A. K., C. Zuffada, and C. Y. Hsieh, "Incoherent bistatic scattering from the sea surface at L-band," *IEEE Trans. Geoscience Remote Sensing,* Vol. 39, 1006–1012, 2001.

5. Kerr, Y. H., P. Waldteufel, J. P. Wigneron, J. M. Martinuzzi, J. Font, and M. Berger, "Soil moisture retrieval from space: the soil moisture and ocean salinity (SMOS) mission," *J. Geophys. Res.,* Vol. 39, No. 8, 1229–1235, 2001.

6. Yueh, S. H., R. West, W. J. Wilson, F. K. Li, E. G. Njoku, and Y. Rahmat-Samii, "Error sources and feasibility for microwave remote sensing of ocean surface salinity," *IEEE Trans. Geosci. Remote Sensing,* Vol. 39, No. 5, 1049–1060, 2001.

7. Saillard, M. and A. Sentenac, "Rigorous solutions for electromagnetic scattering from rough surfaces," *Waves in Random Media,* Vol. 11, R103–R137, 2001.

8. Pak, K., L. Tsang, and J. Johnson, "Numerical simulations and backscattering enhancement of electromagnetic waves from two-dimensional dielectric random rough surfaces with the sparse-matrix canonical method," *J. Opt. Soc. Am. A,* Vol. 14, 1515–1529, 1997.

9. Tran, P., "Calculation of the scattering of electromagnetic waves from a two-dimensional perfectly conducting surface using the method of ordered multiple interaction," *Waves in Random Media,* Vol. 7, 295–302, 1997.

10. Jandhyala, V., B. Shanker, E. Michielssen, and W. C. Chew, "Fast algorithm for the analysis of scattering by dielectric rough surfaces," *J. Opt. Soc. Amer. A,* Vol. 15, 1877–1885, 1998.

11. Li, S.-Q., C.H. Chan, M.-Y. Xia, B. Zhang, and L. Tsang, "Multilevel expansion of the sparse-matrix canonical grid method for two-dimensional random rough surfaces," *IEEE Trans. Antennas Propagat.,* Vol. 47, No. 4, 752–763, April 2001.

12. Torrungrueng, D. and J. T. Johnson, "The forward-backward

method with a novel spectral acceleration algorithm (FB/NSA) for the computation of scattering from two-dimensional large-scale impedance random rough surface," *Microwave Opt. Tech. Letters,* Vol. 29, 232–236, 2001.

13. Soriano, G. and M. Saillard, "Scattering of electromagnetic waves from two-dimensional rough surfaces with impedance approximation," *J. Opt. Soc. Amer. A,* Vol. 18, No. 1, 124–133, 2001.

14. Marvin, A. M. and V. Celli, "Relation between the surface impedance and the extinction theorem on a rough surface," *Phys. Rev. B,* Vol. 50, 14546–14553, 1994.

15. Johnson, J. T., "A numerical study of low-grazing-angle backscatter from ocean-like impedance surfaces with the canonical grid method," *IEEE Trans. Antennas Propagat.,* Vol. 46, 114–120, 1998.

16. Saillard, M. and J. A. DeSanto, "A coordinate-spectral method for rough surface scattering," *Waves Random Media,* Vol. 6, 135–149, 1996.

17. Valenzuela, G. R., "Theories for the interactions of electromagnetic and oceanic waves — a review," *Boundary-Layer Meteorology,* Vol. 13, 61–85, 1978.

18. Yueh, S. H., "Modeling of wind direction signals in polarimetric sea brightness temperatures," *IEEE Trans. Geosci. Remote Sensing,* Vol. 35, No. 6, 1400–1418, 1997.

19. Fung, A. K., *Microwave Scattering and Emission Models and Their Applications,* Artech House, Boston, 1994.

20. Voronovich, G., *Wave Scattering from Rough Surfaces,* Springer-Verlag, Berlin, 1994.

21. Elfouhaily, T., D. R. Thompson, D. E. Freund, D. Vandemark, and B. Chapron, "A new bistatic model for electromagnetic scattering from perfectly conducting surfaces: numerical evaluation and comparison with SPM," *Waves Random Media,* Vol. 11, 33–43, 2001.

22. Milder, D. M., "An improved formalism for electromagnetic scattering from a perfectly conducting rough surface," *Radio Science,* Vol. 31, 1369–1376, 1996.

23. Smith, S., "The operator expansion formalism for electromagnetic scattering from rough dielectric surfaces," *Radio Science,* Vol. 31, 1377–1385, 1996.

24. Alvarez-Perez, J. L., "An extension of the IEM/IEMM surface scattering model," *Waves Random Media,* Vol. 11, 307–329, 2001.

25. Pak, K. P., L. Tsang, C. H. Chan, and J. Johnson, "Backscattering enhancement of electromagnetic waves from two-dimensional perfectly conducting random rough surfaces based on Monte-Carlo simulations," *J. Opt. Soc. Am. A,* Vol. 12, 2491–2499, 1995.

26. Martin, P. A. and P. Ola, "Boundary integral equations for the scattering of electromagnetic waves by a homogeneous dielectric obstacle," *Proc. Roy. Soc. Edinburgh,* Vol. 123, 1993.

27. Ong, T. T., V. Celli, and A. M. Marvin, "General relation between surface impedance and surface curvature," *J. Opt. Soc. Am. A,* Vol. 11, No. 2, 759–765, February 1994.

28. Landau, L. D. and E. M. Lifchitz, *Electrodynamics of Continuous Media,* Pergamon, Oxford, 1982.

29. Johnson, J. T., L. Tsang, R. T. Shin, K. Pak, C. H. Chan, A. Ishimaru, and Y. Kuga, "Backscattering enhancement of electromagnetic waves from two-dimensional perfectly conducting random rough surfaces: a comparison of Monte Carlo Simulations with experimental data," *IEEE Trans. Antennas Propagat.,* Vol. 44, 748–756, 1996.

30. Maystre, D., "Electromagnetic scattering from perfectly conducting rough surfaces in the resonance region," *IEEE Ant. and Prop.,* Vol. 31, 885–895, 1983.

31. Abramovitz, M. and I. E. Stegun (eds.), *Handbook of Mathematical Functions with Formulas, Graphs, and Mathematical Tables,* No. 55 in Applied Mathematics Series, United States Department of Commerce, National Bureau of Standards, Washington D.C., 1991.

32. Tsang, L., J. A. Kong, K. H. Ding, and C. O. Ao, *Scattering of Electromagnetic Waves,* Vol. 2: Numerical Simulations, Wiley-Interscience, New York, 2001.

33. Saillard, M. and D. Maystre, "Scattering from random rough surfaces: a beam simulation method," *Journal of Optics,* Vol. 19, No. 4, 173–176, 1988.

34. Elfouhaily, T., B. Chapron, and K. Katsaros, "A unified directional spectrum for long and short wind-driven waves," *J. Geophys. Res.,* Vol. 102, 15781–15796, July 1997.

35. Klein, L. A. and C. T. Swift, "An improved model for the dielectric constant of sea water at microwave frequencies," *IEEE Trans. Antennas Propagat.,* 1997.

36. Bass, F. G. and I. M. fuks, *Wave Scattering from Statistically Rough Surfaces,* Pergamon, New York, 1979.

37. Brown, G., "Backscattering from a Gaussian-distributed perfectly

conducting rough surface," *IEEE Trans. Antennas Propagat.,* 472–482, 1978.

38. Johnson, J. T., R. T. Shin, J. A. Kong, L. Tsang, and K. Pak, "A numerical study of the composite surface model for ocean backscattering," *IEEE Trans. Geosci. Remote Sensing,* Vol. 36, 72–83, 1998.